

Article

A Multi-Objective Approach to Robust Control of Air Handling Units for Optimized Energy Performance

Mubashir Wani ^{1,*} , Faizal Hafiz ², Akshya Swain ¹ and Abhisek Ukil ¹

¹ Department of Electrical, Computer & Software Engineering, The University of Auckland, Auckland 1010, New Zealand

² SKEMA Business School, Université Côte d'Azur, Sophia Antipolis, 06108 Nice, France

* Correspondence: mubashir.wani@auckland.ac.nz

Abstract: This paper presents a robust control framework with meta-heuristic intelligence to optimize the energy performance of air handling units (AHUs) and to maximize the thermal comfort of occupants by judiciously selecting the temperature set points of two controllers (i.e., the H_∞ controller and the boiler controller). The selection of these set points is formulated as a *multi-objective optimization problem*, where the goal is to balance *energy consumption* with *thermal comfort*. Furthermore, the uncertainty weights of the H_∞ controller are estimated to minimize oscillations in the *outflow air temperature* of the AHU plant. The performance of the proposed framework is investigated by considering the real-time weather data of Auckland, New Zealand. The results of the simulation show that the proposed robust control framework could significantly reduce oscillations in the outflow air temperature compared with the conventional case, where the temperature set points are selected empirically. Moreover, annual energy savings of 49.13% are achieved without compromising the thermal comfort.

Keywords: air handling units; energy consumption; multi-objective optimization; occupant comfort; set points



Citation: Wani, M.; Hafiz, F.; Swain, A.; Ukil, A. A Multi-Objective Approach to Robust Control of Air Handling Units for Optimized Energy Performance. *Electronics* **2023**, *12*, 661. <https://doi.org/10.3390/electronics12030661>

Academic Editors: Akira Otsuki and Pezhman Ghadimi

Received: 27 December 2022

Revised: 24 January 2023

Accepted: 26 January 2023

Published: 28 January 2023



Copyright: © 2023 by the authors. Licensee MDPI, Basel, Switzerland. This article is an open access article distributed under the terms and conditions of the Creative Commons Attribution (CC BY) license (<https://creativecommons.org/licenses/by/4.0/>).

1. Introduction

The demand for energy consumption has been increasing at an alarming rate with the increase in world population. To meet this increasing energy demand, a large dependence of the world over the past decade or so has been *non-renewable energy resources*. This trend is more likely to remain the same in the foreseeable future, even though heavy investments are currently being made in the *renewable energy* sector. The complication is that the availability of non-renewable resources is scarce. The rate at which they are being consumed presently will make them insufficient for the increasing energy demand in the future. Moreover, their increasing use is also posing a detrimental impact on the Earth's environment, which includes climate change (global warming), rising sea levels and so on. To become independent from the use of non-renewable resources seems to be feasible. However, this will not be dynamic, as it would take several decades to free ourselves from the use of non-renewable energy resources and completely switch to renewable energy resources [1]. Meanwhile, efficient utilization of the available energy resources can be regarded as a highly capable substitute to address the aforementioned problems, as this will prompt a reduced rate of non-renewable resource consumption [2]. The latest statistical data released by U.S Energy Information Administration (EIA) indicates that over 40% of the energy produced from the world's resources is consumed by the buildings sector alone, with residential and commercial buildings included, and more than one-third of this energy consumed is utilized for space heating and cooling [3,4]. These statistics give a strong implication that minimizing the energy usage of heating, ventilation and air conditioning (HVAC) systems can be a principal element in realizing the curtailment of world's energy

consumption and, consequently, global climate change. A need for optimizing the operation of HVAC systems is thus certain in order to minimize their overall uptime and energy consumption in buildings, but this should be realized such that the thermal comfort of the occupants is minimally affected. Maintenance of a comfortable environment for occupants is critically acknowledged as one of the important goals in smart and energy-efficient buildings [5,6]. Some of the factors which are fundamental in realizing the occupants' overall comfort in a building environment include thermal comfort, air quality and visual comfort [7]. Realization of improvement in any of these comfort factors results in higher building energy consumption. One of the principal issues in building energy management systems (BEMS) is therefore to create a balance between two *objectives: occupants' thermal comfort and energy consumption*.

In the past few decades, several useful energy management systems (EMS) have been proposed for optimized energy performance and thermal comfort management in buildings [7] using various control methods such as model predictive control (MPC) [8] and robust control [9]. In order to guarantee thermal comfort to the occupants, it is necessary to ensure minimal oscillations in the heating, ventilation and air conditioning (HVAC) plant output so that the desired set point values can be realized within stipulated time steps [10]. To this end, controllers based on modern control methods, such as H_∞ , have been used in the past in HVAC control applications [11–13]. For instance, in [11], Underwood designed an H_∞ -based robust controller for an HVAC plant by considering the nominal linear model, wherein the focus is on minimization of the oscillations in the outflow air temperature of the plant. Although the controller proposed in [11] performs well under *design load* conditions, it manifests oscillatory behavior in *half* and *quarter load* conditions. Such performance is often undesirable from both the thermal comfort and energy consumption points of view.

The controllers discussed above are essentially based on the concept of classical feedback control. It has been acknowledged that in order to have an effective thermal control system (strategy) in buildings, it should account for both of the above objectives (i.e., thermal comfort and energy consumption) simultaneously under all operating conditions [14,15]. To address this issue, many researchers in the area of smart BEMS have formulated the problem from a multi-objective optimization (MOO) perspective [16–20] where, in general, the concept of classical feedback control is integrated with *heuristics*. For instance, Jindal et al. [19] proposed an energy management scheme for controlling the HVAC systems in the classrooms of a university building, wherein a heuristic algorithm was proposed to optimally schedule the usage of HVAC. The results of the work indicated a 19.75% reduction in the energy demand by HVAC systems for an entire week without affecting the thermal comfort of the occupants. However, the nonlinear nature of the HVAC system was not taken into account. In [10], the problem of maximizing the energy efficiency of HVAC systems was formulated as a nonlinear optimization problem and solved using the particle swarm optimization (PSO) technique. Wang et al. [20] proposed a multi-agent framework with heuristic intelligence for optimizing the overall occupant comfort and energy consumption in buildings. However, the influence of varying weather conditions, which are often responsible for causing heavy oscillations in an HVAC system's output, was not considered. Some other recent research where multi-objective techniques have been utilized with a focus on HVAC systems in particular can be found in [21–25]. For instance, in [22], a convex programming (CP)-based DR optimization framework is presented for the load management of various household appliances through BEMS in a *smart home*. This work primarily targets the objectives which focus on optimizing the energy performance of HVAC systems. A *multi-objective mixed-integer linear programming (MOMILP)-based framework* was proposed in [24] to *minimize building energy consumption*. Furthermore, Li et al. [25] formulated an MOO problem for *minimizing the operational costs* of the utility, along with *maximizing DR aggregators' and users' benefits*. All the research mentioned and discussed above address very significant aspects of energy and comfort management in buildings. However, relatively less evidence could be found in the literature, where

the nonlinear nature of the HVAC system model is considered along with focus on the balancing of energy consumption and comfort.

In the present study, a novel robust control framework is proposed which focuses on optimization of the energy performance of an air handling unit (AHU) while maintaining better occupant thermal comfort. This is achieved by effectively controlling the outflow air temperature of the AHU via two different controllers: an H_∞ controller and a boiler controller. The performance of these controllers is critically determined by the set points (reference signals). Therefore, in the proposed framework, the selection of these set points to the controllers is formulated as a multi-objective optimization problem, wherein the goal is to balance the energy consumption of the AHU with the thermal comfort. In the optimization process, the optimal set points to these controllers are computed (in accordance with the occupant's specified comfort parameters) using a well-known meta-heuristic: NSGA-II [26–28]. Some highlights of the proposed framework and main contributions of this paper are summarized as follows:

- 1 A key aspect of our framework is that the multi-objective optimization is performed *online*, (i.e., the optimal set points are computed while considering the time-varying weather data of Auckland, New Zealand in real time during the simulations).
- 2 To reduce the computation time per time step and to expedite the online optimization process, an approximation scheme is developed to estimate the *water mass flow rate* (an important variable in one of the objective functions). This reduces the complexity of the proposed framework as well.
- 3 A nonlinear thermal model of a typical AHU plant [29,30] is used as a benchmark to validate the performance of the proposed framework.
- 4 During the optimization process, an a posteriori approach is used to select the *knee point* solution from the pool of evaluated non-dominated optimal solutions. This ensures a proper balance between *minimization of energy consumption* and *maintenance of thermal comfort*.
- 5 The uncertainty weights of the H_∞ controller are estimated to reduce oscillations in the outflow air temperature of the AHU plant.

The remainder of this paper is organized as follows. Section 2 provides a brief description of the AHU plant model considered in this study. Section 3 explains the problem formulation. The structure of the control system is discussed in Section 4, followed by the simulation results and conclusions in Sections 5 and 6, respectively.

2. Dynamic Model of the AHU Plant

The dynamics of the AHU plant (see Figure 1) derived from the first principles and considered in this study are given by [29].

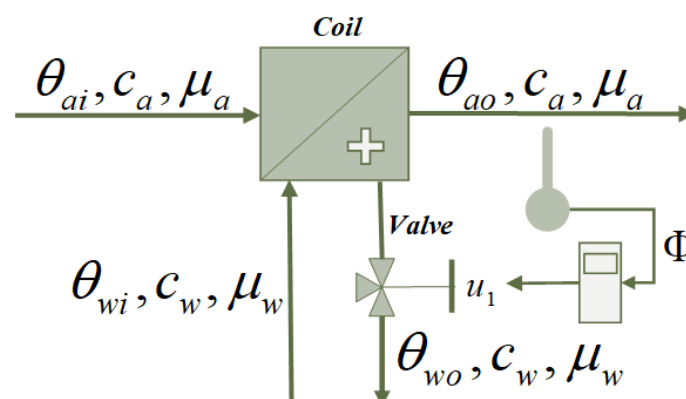


Figure 1. Schematic of the heating coil unit (HCU) of the AHU.

$$\begin{aligned}
C_w \dot{\theta}_{wo} &= \mu_w c_w (\theta_{wi} - \theta_{wo}) - Q_w \\
C_m \dot{\theta}_m &= Q_w - Q_a \\
\text{where, } Q_w &= U_w A_w (\theta_{wo} - \theta_m) \\
Q_a &= U_a A_a (\theta_m - \theta_{ao})
\end{aligned} \tag{1}$$

where C_w and C_m denote the thermal capacities of water and the heat exchanger material, respectively, θ_{wo} , θ_{wi} , θ_m and θ_{ao} are the outflow water, inflow water, heat exchanger material and outflow air temperatures, respectively, Q_w and Q_a represent the heat transfer rates of water and air, respectively, U_w and U_a denote the thermal transmission coefficients of water and air, respectively, μ_w represents the water mass flow rate and c_w is a constant ($4.194 \text{ kJ}\cdot\text{kg}^{-1}\cdot\text{K}^{-1}$) denoting the specific heat capacity of water.

Assuming an instantaneous heat transfer between the air and the heating coil, we have

$$Q_a = \mu_a c_a (\theta_{ao} - \theta_{ai}) \tag{2}$$

where μ_a denotes the air mass flow rate, c_a is a constant ($1.002 \text{ kJ}\cdot\text{kg}^{-1}\cdot\text{K}^{-1}$) denoting the specific heat capacity of air and θ_{ai} represents the inflow air temperature.

From the expression of Q_a given in Equations (1) and (2), we have

$$\theta_{ao} = \frac{\mu_a c_a \theta_{ai} + U_a A_a \theta_m}{\mu_a c_a + U_a A_a} \tag{3}$$

The thermal transfer coefficient on the water side of the coil for the turbulent-forced convection (heavy thermal load) U_w is given by

$$\begin{aligned}
U_w &= (5.823 + 1.153 \times 10^{-1} \theta_{wo} - 1.48 \times 10^{-4} \theta_{wo}^2) \\
&\times \left[\frac{\mu_w}{n_{tb} d_i^{2.25}} \right]^{0.8}
\end{aligned} \tag{4}$$

and for the laminar forced convection (light thermal load), we have

$$\begin{aligned}
U_w &= \frac{4.36}{d_i} \times (0.5702 + 1.79 \times 10^{-3} \bar{\theta}_m \\
&\quad - 6.7714 \times 10^{-6} \bar{\theta}_{wm}^2) \\
\text{where } \bar{\theta}_{wm} &= \frac{\theta_{wo} + \theta_m}{2}
\end{aligned} \tag{5}$$

Equations (4) and (5) represent a sharp edge, but the transition between the turbulent and laminar flow of liquid is gradual. For this purpose, the transition between the two has been relaxed as follows:

$$U_w = \max(U_w|_{Re \geq 2300}, U_w|_{Re < 2300}) \tag{6}$$

The thermal transfer coefficient on the air side of the coil U_a is given by

$$U_a = 60.37 + 140.3 \times \exp\left(\frac{28.62 - \theta_m}{9.796}\right) \tag{7}$$

Furthermore, assuming that the hysteresis due to the actuator linkage mechanism is negligible within the control valve, the mass flow rate of the water flowing through the coil can be represented as follows:

$$\tau_a \dot{\mu}_w = \Psi \mu_{wd} - \mu_w \tag{8}$$

where

$$\Psi = \gamma \times [\gamma^2 (1 - \mathcal{N}) + \mathcal{N}]^{-\frac{1}{2}} \tag{9}$$

Since equal percentage characteristics are assumed for the control valve, we have

$$\gamma = f_o^{(1-u_1)} \tag{10}$$

A first-order representation is also assumed for the temperature sensor:

$$\tau_s \dot{\Phi} = \theta_{ao} - \Phi \tag{11}$$

3. Problem Formulation

The present study proposes a meta-heuristic based framework for robust control of the outflow air temperature θ_{ao} of a typical AHU plant (see Figure 1). Herein, the prime goal is to achieve two objectives simultaneously: (1) minimization of AHU plant energy consumption by reducing the thermal load on the AHU and (b) maximization of thermal comfort by reducing the oscillations in the AHU plant output θ_{ao} . To this end, two different controllers, an H_∞ controller and a boiler controller, are used to control the outflow air temperature of the AHU plant (discussed in Section 4). The performance of these controllers is critically determined by the reference signals (set points) θ_{ao}^{ref} and θ_{wi}^{ref} . Therefore, the goal in this work is to determine the optimal values of these reference signals using a suitable multi-objective optimization technique such that the above two conflicting objectives are balanced.

Let us consider the p th solution set Θ^p :

$$\Theta^p = [\theta_1^p, \theta_2^p] \tag{12}$$

where θ_1 and θ_2 are being used to represent θ_{ao}^{ref} and θ_{wi}^{ref} , respectively, for the sake of simplicity. The superscript p represents the p th candidate solution set (particle) from the optimization technique (PSO) used in this paper. Hence, θ_1^p denotes the candidate outflow air temperature set point, and θ_2^p denotes the candidate inflow water temperature set point. These form the decision variables in the optimization process. The goal of the optimization task is to evaluate the optimal solution set (i.e., $\Theta^* (= [\theta_{ao}^*, \theta_{wi}^*] \text{ or } [\theta_1^*, \theta_2^*])$) as shown below:

$$\Theta^* = \underset{\forall \Theta^p \in \Theta_{dom}}{\text{arg min}} \begin{cases} J_1(\Theta^p) \\ J_2(\Theta^p) \end{cases} \tag{13}$$

where $\Theta_{dom} = [\Theta_{min}, \Theta_{max}]$ represents the search domain of the decision variables to be specified by the decision maker (occupant). The objective functions $J_1(\cdot)$ and $J_2(\cdot)$ are mathematically expressed as follows:

I. Energy function:

$$J_1(\Theta^p) = 1 - \delta \left(1 - \left(\frac{\theta_1^p - \theta_{ai}}{\theta_1^p} \right)^2 \right) \tag{14}$$

where δ is an occupant-specified parameter (to be called the energy index) which determines the amount of thermal load on the AHU plant. It is worth emphasizing here that the energy consumption of the AHU plant is determined by the thermal load, which is influenced by the difference between the outside temperature θ_{ai} and the set-point (i.e., θ_1^p). Thus, the smaller this temperature difference, the smaller the thermal load on the AHU plant is.

II. Discomfort function:

$$J_2(\Theta^p) = \left| \frac{\theta_{ao} - \theta_1^p}{\theta_1^p} \right| \text{ where,} \tag{15}$$

$$\theta_{ao} = \frac{\mu_w c_w}{\mu_a c_a} (\theta_2^p - \theta_1^p) + \theta_{ai}$$

The corresponding comfort level is calculated as follows:

$$Comfort = 1 - J_2(\Theta^p) \tag{16}$$

For the above expression of θ_{ao} , refer to Section 3.1. Note that the occupants’ thermal discomfort is determined by the difference between the outflow air temperature θ_{ao} and the set point θ_1^p . As this temperature difference decreases, the discomfort level of the occupants decreases (i.e., the comfort level increases).

For the p th candidate’s solution, at the k th time step (i.e., Θ_k^p), the objective functions $J_1(\cdot)$ and $J_2(\cdot)$ are evaluated as per Algorithm 1. It should be noted that for better functionality of the method, both objectives $J_1(\cdot)$ and $J_2(\cdot)$ are normalized (see Algorithm 1 (Line 11)).

Algorithm 1: Evaluation of objective functions at the k th time step.

```

Input : Search Agent,  $\Theta_k^p = \{\theta_1^p(k), \theta_2^p(k)\}$ ; Outside Weather Profile,  $\mathcal{W}$ ; Energy Index,  $\delta$ ,
        AHU Plant Output,  $\theta_{ao}(k-1)$ 
Output: Objective values:  $J_1(\cdot)$  and  $J_2(\cdot)$ 

*/   Outside Sensor (temperature) data
1 Collect the outside temperature value, i.e.,  $\theta_{ai}(k) \leftarrow \mathcal{W}$ ,  $k = 1, 2, \dots, N$ 
*/   Evaluate the Objective Functions

*/   Intuitive energy consumption level
2  $J_1(\Theta_k^p) \leftarrow 1 - \delta \left( 1 - \left( \frac{\theta_1^p(k) - \theta_{ai}(k)}{\theta_1^p(k)} \right)^2 \right)$ 
*/   Approximate Mass-flow Rate,  $\mu_w(k)$ 
3 Calculate error (see Figure 2);  $e(k) \leftarrow \theta_1^p(k) - \theta_{ao}(k-1)$ 
*/   Compute Robust Controller Output,  $u_1(t)$ 
4 for  $t = t_0$  to  $t_{final}$  do
5    $u_1(t) \leftarrow f(K(s), e(k), t)$ 
6 end
7  $\gamma \leftarrow f_o^{1-u_1(t_{final})}$ 
8  $\mu_w(k) \approx \mu_{wd} \times \gamma \times [\gamma^2(1 - \mathcal{N}) + \mathcal{N}]^{-\frac{1}{2}}$ 
*/   Approximate  $\theta_{ao}(k)$ 
9  $\theta_{ao}(k) \approx \frac{\mu_w(k)c_w}{\mu_a c_a} (\theta_2^p(k) - \theta_1^p(k)) + \theta_{ai}(k)$ 
*/   Occupant discomfort level,  $J_2(\cdot)$ 
10  $J_2(\Theta_k^p) \leftarrow \left| \frac{\theta_{ao}(k) - \theta_1^p(k)}{\theta_1^p(k)} \right|$ 
*/   Normalize  $J_1(\cdot)$  and  $J_2(\cdot)$  between [0,1]
11  $J_1(\cdot) \leftarrow \frac{J_1(\cdot) - J_{1,min}}{J_{1,max} - J_{1,min}}$ ;  $J_2(\cdot) \leftarrow \frac{J_2(\cdot) - J_{2,min}}{J_{2,max} - J_{2,min}}$ 

```

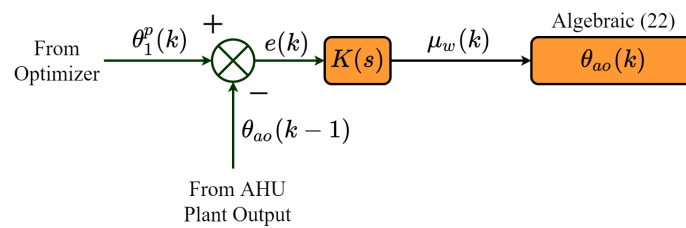


Figure 2. Approximation approach to evaluating Equation (22).

3.1. Approximation Approach to Evaluate θ_{ao}

Since AHU plants are characterized by slower dynamics, it can be assumed at a given instant that

$$\dot{\theta}_{wo} \approx 0; \quad \dot{\theta}_m \approx 0 \tag{17}$$

Based on this assumption, from Equation (1), we have

$$Q_w = \mu_w c_w (\theta_{wi} - \theta_{wo}) \quad \text{and} \quad Q_w \approx Q_a \tag{18}$$

Furthermore, from Equations (2) and (18), we have

$$\begin{aligned} \mu_a c_a (\theta_{ao} - \theta_{ai}) &\approx \mu_w c_w (\theta_{wi} - \theta_{wo}) \\ \frac{\mu_w c_w}{\mu_a c_a} (\theta_{wi} - \theta_{wo}) &\approx \theta_{ao} - \theta_{ai} \\ \theta_{ao} &\approx \frac{\mu_w c_w}{\mu_a c_a} (\theta_{wi} - \theta_{wo}) + \theta_{ai} \end{aligned} \tag{19}$$

Under ideal conditions, it can be assumed that

$$\theta_{ao} \approx \theta_{wo} \approx \theta_{ao}^{ref} \quad \text{and} \quad \theta_{wi} \approx \theta_m \approx \theta_{wi}^{ref} \tag{20}$$

Using Equation (20) in Equation (19), θ_{ao} can thus be represented as follows:

$$\theta_{ao} \approx \frac{\mu_w c_w}{\mu_a c_a} (\theta_{wi}^{ref} - \theta_{ao}^{ref}) + \theta_{ai} \tag{21}$$

For the p th solution set (i.e., $\Theta^p (= [\theta_1^p, \theta_2^p])$), we have

$$\theta_{ao} \approx \frac{\mu_w c_w}{\mu_a c_a} (\theta_2^p - \theta_1^p) + \theta_{ai} \tag{22}$$

where $c_w = 4.194 \text{ kJ}\cdot\text{kg}^{-1}\cdot\text{K}^{-1}$, $c_a = 1.002 \text{ kJ}\cdot\text{kg}^{-1}\cdot\text{K}^{-1}$ and $\mu_a = 0.3144 \text{ kg}\cdot\text{s}^{-1}$ are all constants.

It is worth mentioning here that the ideal goal of the optimization task is to minimize $J_1(\cdot)$ and $J_2(\cdot)$. However, these objectives are conflicting and cannot be minimized simultaneously in practice. Therefore, the goal is to search for the best possible solution which balances (satisfies) both objectives $J_1(\cdot)$ (energy function) and $J_2(\cdot)$ (discomfort function).

To this end, the framework comprises the following two processes.

3.2. Search Process

The principal step in the optimization process is to formulate an effective search strategy to find the optimal solution set, which in this case is Θ^* (see Equation (13)). In this study, a multi-objective evolutionary algorithm (MOEA) called Non-Dominated Sorting Genetic Algorithm II (NSGA-II) is used for this purpose because of its popularity and efficiency in solving multi-objective optimization problems. NSGA-II is a seminal dominance-based MOEA which utilizes dominance-based relations for ranking and segregating the entire population of solutions into successive fronts using a well-known non-dominated sorting operation. Implementation and other details pertaining to NSGA-II are out of the scope of this paper and can be found elsewhere [31,32]. Although there are several *multi-objective*

evolutionary algorithms (MOEAs) which are suitable for the task, such as *Multi-Objective Particle Swarm Optimization (MOPSO)*, the *Pareto Archived Evolution Strategy (PAES)* and the *Strength Pareto Evolutionary Algorithm (SPEA)*, this study considered the use of *Non-Dominated Sorting Genetic Algorithm -II (NSGA-II)*. The rationale behind utilizing NSGA-II in this work is that it has been proven to perform well for solving *multi-objective optimization problems (MOOPs)* [33]. Further, NSGA-II is also known to be computationally better than its previous version (i.e., NSGA), apart from being able to give comparable performance to that of its two contemporary MOEAs (i.e., PAES and SPEA) [32,34].

In the framework, each search agent in NSGA-II represents a candidate solution set Θ^p , the performance of which is evaluated as per the steps outlined in Algorithm 1. Note that the optimization process is performed online, and therefore for the p th candidate solution at the k th time step (i.e., Θ_k^p), the objective functions $J_1(\cdot)$ and $J_2(\cdot)$ are evaluated:

$$J_1(\Theta_k^p) = 1 - \delta \left(1 - \left(\frac{\theta_1^p(k) - \theta_{ai}(k)}{\theta_1^p(k)} \right)^2 \right) \tag{23}$$

$$J_2(\Theta_k^p) = \left| \frac{\theta_{ao}(k) - \theta_1^p(k)}{\theta_1^p(k)} \right| \tag{24}$$

Due to the stochastic nature of NSGA-II, the best solution sets Θ_r^* evaluated over multiple independent algorithm runs (denoted by R), are considered at every single time step k (see Algorithm 2 (Lines 2–5)).

Algorithm 2: Meta-heuristic solution set selection.

Input : Search Domain, Θ_{dom}
Output: Optimized Solution-set, $\Theta^* = [\theta_1^*, \theta_2^*]$

```

*/      Time-steps
1 for k = 1 to N do
    */      'R' independent runs of NSGA-II
2      $\Pi \leftarrow \emptyset, \quad \Gamma \leftarrow \emptyset$ 
3     for r = 1 to R do
        */      Store the approximate Pareto solutions
4          $\Pi \leftarrow \{\Pi \cup \Theta_r^*\}, \quad \Gamma \leftarrow \left\{ \Gamma \cup [J_1(\Theta_r^*), J_2(\Theta_r^*)] \right\}$ 
5     end
        */      Keep only the non-dominated solutions
6      $\Gamma^* \prec \Gamma, \Pi^* \prec \Pi$ 
        */      A posteriori selection
7     Select the knee-point solution set,  $\Theta_k^* \in \Pi^*$ , using MMD approach [26]
8      $\theta_1^*(k) \rightarrow H_\infty$  controller reference &  $\theta_2^*(k) \rightarrow$  boiler controller reference; at kth
        time-step.
9 end

```

3.3. Best Solution Selection Process

After all the runs are complete, the non-dominated solutions over R -runs are treated as the Approximate Pareto Front (APF) (i.e., Π^*). Subsequently, the optimal set points $\theta_1^*(k)$ and $\theta_2^*(k)$ are selected from the APF by following the steps outlined in Lines 6 and 7 of Algorithm 2. Since the premise of this work is based on creating a balance between the

above two objectives, an a posteriori selection approach called the minimum Manhattan distance (MMD) was adopted to select a knee point solution from the APF [26–28]. To this end, the Manhattan distance $D(\cdot)$ was determined between the hypothetical ideal point z_0^{ideal} and each non-dominated solution in the APF Π^* . Following this, the solution corresponding to the minimum distance $D(\cdot)$ was selected:

$$\Theta^* = \left\{ \Theta_j \mid D(\Theta_j) = \arg \min D(\Theta_j), \forall \Theta_j \in \Pi^* \right\} \tag{25}$$

where $\Theta_j \in \Pi^*$ denotes the j th non-dominated solution in the APF Π^* . Finally, the identified knee point solutions (i.e., $\Theta^* = \{\theta_1^*(k), \theta_2^*(k)\}$) are sent to the H_∞ and the boiler controllers, respectively.

4. Structure of the Control System

The structure of the control system is shown in Figure 3. In particular, the two controllable inputs u_1 and u_2 of the AHU plant are controlled via the H_∞ controller $K(s)$ and the boiler controller, respectively. Moreover, to achieve the objectives described in Section 3, the system consists of an optimizer which has two parts: Part I and Part II. The purpose of Part I is to utilize the outside environmental information (i.e., the dry-bulb temperature θ_{ai}) collected by outside sensor and the occupant-specified comfort parameters to determine the optimal (best) temperature set point θ_{ao}^* at each time step. This optimized set point is received by the H_∞ controller, which controls the water mass flow rate μ_w flowing through the AHU coil by controlling the fractional valve-stem position F for temperature control. Part II of the optimizer focuses on controlling the inflow water temperature θ_{wi} of the AHU plant. Note that the dead time (delay) between the inflow water temperature θ_{wi} delivered by the boiler control system and the set point θ_{wi}^* evaluated by our algorithm was assumed to be negligible (i.e., at a given time instant, $\theta_{wi} \approx \theta_{wi}^*$).

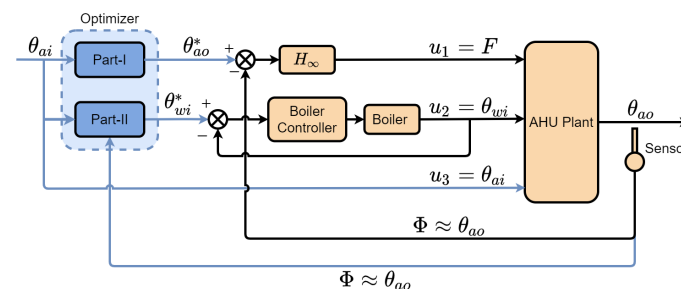


Figure 3. Structure of control system.

The design of the H_∞ controller followed similar procedure to that given in [11], and it is therefore discussed briefly here for the sake of completeness.

Initially, the outflow air temperature θ_{ao} of the AHU plant is generated via simulations from its nonlinear model (described in Section 2). The values of the parameters of the model used in the simulation can be found in [29]. A first-order lag plus delay linear time-invariant (LTI) model is fitted to this data:

$$G(s) = g_{pt} \times \frac{\exp(-\Delta_{pt}s)}{(\tau_{pt}s + 1)} \tag{26}$$

The uncertainty bounds of various terms of the model in Equation (26) are determined by curve fitting and are given as $[g_{pt}^-, g_{pt}^+] = [8.9 \text{ K}, 48.4 \text{ K}]$, $[\Delta_{pt}^-, \Delta_{pt}^+] = [23.3 \text{ s}, 41.3 \text{ s}]$ and $[\tau_{pt}^-, \tau_{pt}^+] = [47.9 \text{ s}, 61.5 \text{ s}]$. Note that these bounds reflect the structural uncertainties of the model which are considered during the design of the H_∞ controller.

The uncertainty in the gain (g_{pt}) and time delay (Δ_{pt}) parameters are used to derive the uncertainty weights, which consist of an integrator for performance (W_1) and first-order lead lag for the model uncertainty (W_3), resulting in a fifth-order augmented plant description. Note that the controller weight (W_2) has been neglected in this design, the reason for which is explained well in [11]. The resulting augmented plant model is used to develop a robust controller (K) which minimizes the H_∞ norm of the closed-loop plant (based on the solution of 2-Riccati algebraic equations), which is given as follows:

$$\min_K \left\| \begin{matrix} W_1 S \\ W_2 K S \\ W_3 T \end{matrix} \right\|_\infty \tag{27}$$

where S and T denote the normalized and complementary sensitivity functions, respectively. The transfer function of the stabilizing H_∞ controller is given as

$$K(s) = \frac{2.69s^4 + 3.51s^3 + 0.87s^2 + 0.054s + 0.008}{s^5 + 4.48s^4 + 8.04s^3 + 5.27s^2 + 0.712s} \tag{28}$$

Note that in this work, the set point θ_1^* (i.e., θ_{ao}^*) varied after every 600 s as per the outside temperature (discussed in Section 5) θ_{ai} . Thus, the purpose of the H_∞ -based controller was to maintain stability and performance of the AHU in all operating conditions by regarding the varying optimal set point θ_1^* (i.e., θ_{ao}^*) as a disturbance.

5. Simulation Results and Discussion

The efficacy of the proposed framework in balancing the two conflicting objectives was investigated via simulations in a MATLAB®/Simulink® environment, considering the real-time weather profile of Auckland City. This was obtained from the meteorological data provided by the National Institute of Water and Atmospheric Research Limited (NIWA) in New Zealand [35].

5.1. Simulation Set-Up

The optimization was carried out online, where the objective functions $J_1(\cdot)$ and $J_2(\cdot)$, corresponding to the p th candidate solution set at the k th time step (i.e., Θ_k^p), were evaluated as per Equations (23) and (24), respectively. Note that the value of the energy index δ was in the range of [0, 1]. In this work, δ is assumed to be one (i.e., minimizing the thermal load is assigned the highest priority).

The search domain Θ_{dom} used in this study is shown in Table 1. This was in compliance with the operative room temperatures recommended by the ASHRAE standard [36] (i.e., 20–23 °C during winter and 23–25 °C during summer). It is worth noting that the thermal comfort range (i.e., $[\theta_1^{min}, \theta_1^{max}]$) and the energy index δ were occupant (decision maker)-specified parameters and were key in evaluating the optimal (knee point) solutions θ_1^* (i.e., θ_{ao}^*) and θ_2^* (i.e., θ_{wi}^*).

The optimization was performed using the NSGA-II algorithm (see Section 3.2). To accommodate the stochastic nature of the NSGA-II algorithm, a total of 10 independent runs were carried out at each time step. Furthermore, single-point crossover was used as the recombination mechanism with the following crossover and mutation probabilities: $\{p_c, p_m\} = \{0.7, 0.05\}$. Each run of NSGA-II was terminated after 5000 function evaluations (FEs), and the population size ps was fixed at 50.

Table 1. Search domain of decision variables.

Decision Variable	Search Domain (Θ_{dom})	
	Min	Max
θ_1 (°C)	19	25
θ_2 (°C)	10	40

5.2. Performance Evaluation of the H_∞ Controller without the Optimizer

Initially, the H_∞ controller (described in Section 4) was designed to control the outflow air temperature θ_{ao} by varying u_1 (see Figure 4). Without loss of generality, the investigation was carried out while considering both a notional periodic square waveform and a step signal as the reference (i.e., θ_{ao}^{ref}) to the H_∞ controller. Note that the AHU plant dynamics here were simulated for a duration of 4000 s (using square wave input) and 1000 s (using step input), respectively, at a sampling interval of 1 ms. Furthermore, the reference of the boiler controller θ_{wi}^{ref} was chosen to be 28 °C. The output of the AHU plant (θ_{ao}) and the corresponding comfort level for these reference inputs are shown in Figures 5 and 6 for three specific thermal load conditions. It was observed that the output of the AHU exhibited highly oscillatory behavior, particularly under part-load conditions, which resulted in a decreasing comfort level. Consequently, the power consumed by the AHU plant over a given duration also showed high oscillatory behavior with significant overshoots (see Figures 7 and 8). Note that these observations are inline and consistent with the earlier investigations in [29], wherein similar oscillatory behavior was also observed under part-load conditions. Thus, the reference signals to the H_∞ controller and the boiler controller shall be judiciously selected to achieve better comfort with less energy consumption.

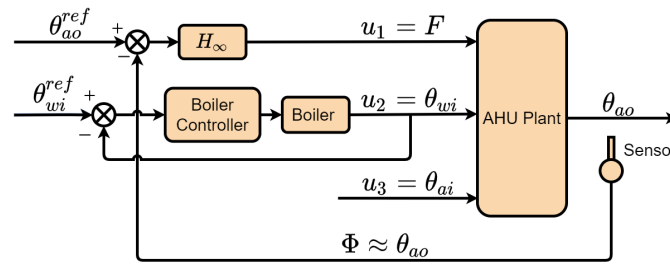


Figure 4. Illustration of conventional control of θ_{ao} .

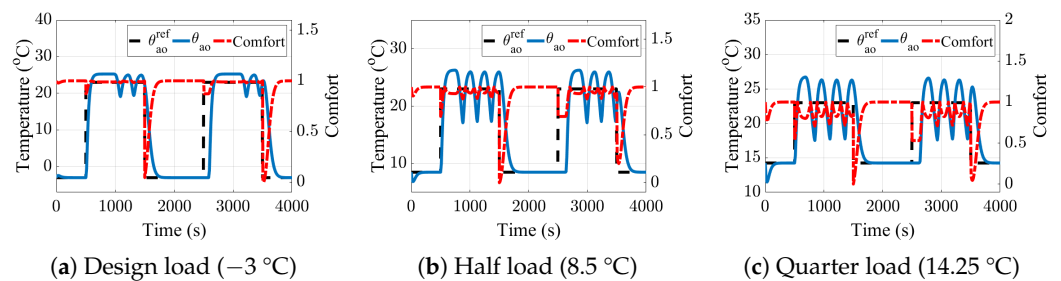


Figure 5. AHU plant response with H_∞ controller at three different thermal load conditions (square wave input).

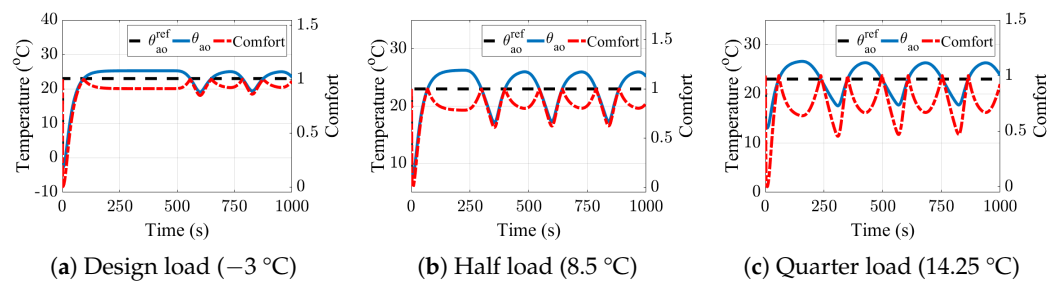


Figure 6. AHU plant response with H_∞ controller at three different thermal load conditions (step input).

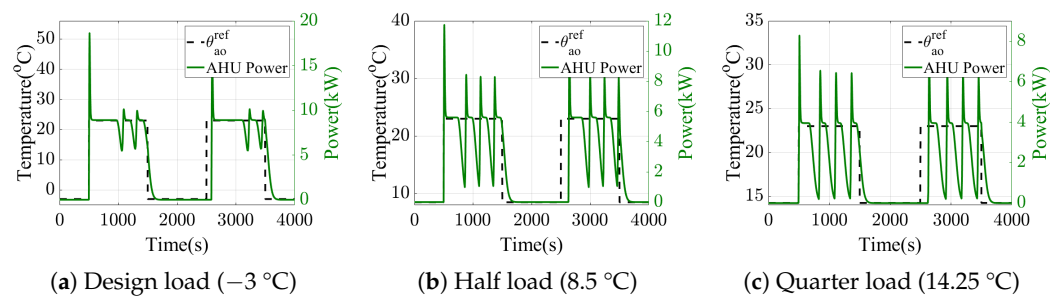


Figure 7. AHU system power consumption with H_{∞} controller at three different thermal load conditions (square wave input).

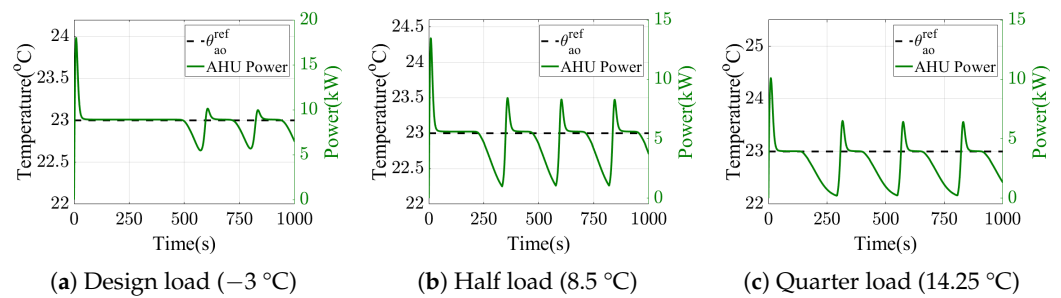


Figure 8. AHU system power consumption with H_{∞} controller at three different thermal load conditions (step input).

5.3. Performance Evaluation of the H_{∞} Controller with the Optimizer

Following the simulation set-up described in Section 5.1 and the procedures explained in Section 3, the final output from the optimizer (i.e., the knee point solution(s) $\Theta^* (= [\theta_{ao}^*, \theta_{wi}^*])$), were used as reference signals for the controllers, which controlled the fractional valve-stem position u_1 , and the inflow water temperature u_2 of the AHU plant (see Figure 3). To supplement the understanding of this, Figures 9 and 10 show the Pareto optimal fronts and the corresponding knee point solutions determined by our algorithm at four different outside temperatures θ_{ai} .

It is worth mentioning that the AHU plant dynamics here were simulated while considering the Auckland weather profile data for the entire year (i.e., for a duration of 8640 h and with a sampling interval of 1 ms). Further, given that the slower dynamics tend to dominate the plant performance in HVAC system control, the set points were optimized at an interval of 10 min (i.e., the optimizer was operating at a step size of 600 s). For brevity purposes, we presented the performance of the H_{∞} controller with the proposed optimizer during a typical warm and a cool day in Figures 11 and 12, respectively. Figure 11a shows the variation of optimized set points θ_{ao}^* and θ_{wi}^* evaluated by the optimizer in accordance with the inflow air temperature θ_{ai} (i.e., outside air temperature). It is worth noting that there was a huge fluctuation in the optimized inflow water temperature set point θ_{wi}^* over time, particularly between 12:00 a.m. and 8:00 a.m. The reason for this was based on the working mechanism of the AHU plant (see Figure 1). In particular, the main variables which controlled the outflow air temperature θ_{ao} were the fractional valve-stem position u_1 and the inflow water temperature θ_{wi} . During the time between 12:00 a.m. and 8:00 a.m., the outside temperature θ_{ai} was recorded to be the minimum, and as a result, the optimizer pushed the value of the optimized set point θ_{wi}^* higher to keep the value of θ_{ao} within the defined comfort range [19 °C, 25 °C] as per our proposed framework (see Table 1). Similar behavior can be observed in the trend of θ_{wi}^* in Figure 12a, which was simulated for a day during the winter season. It can be observed that the H_{∞} controller with the optimizer (see Figure 3) was able to minimize the energy consumption compared with the H_{∞} controller without the optimizer (see Figure 4). Furthermore, this controller with the optimizer could maintain the occupant comfort at a higher level.

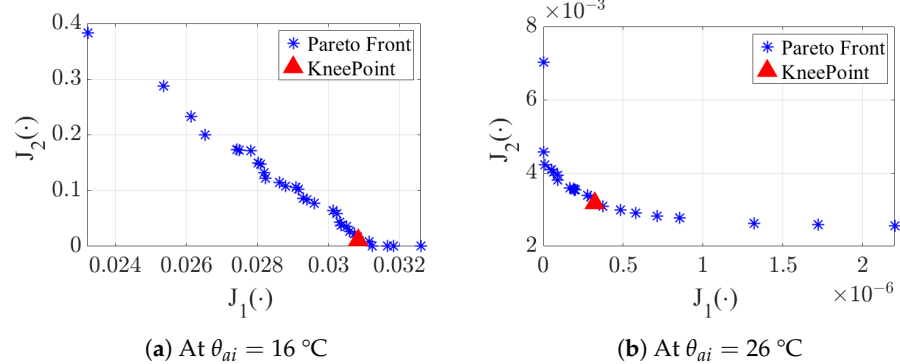


Figure 9. Pareto optimal fronts generated at minimum (16 °C) and maximum (26 °C) outside temperatures θ_{ai} recorded during summer.

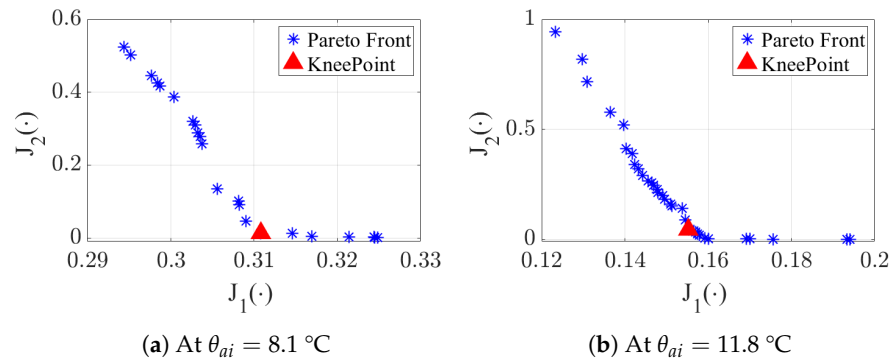


Figure 10. Pareto optimal fronts generated at minimum (8.1 °C) and maximum (11.8 °C) outside temperatures θ_{ai} recorded during winter.

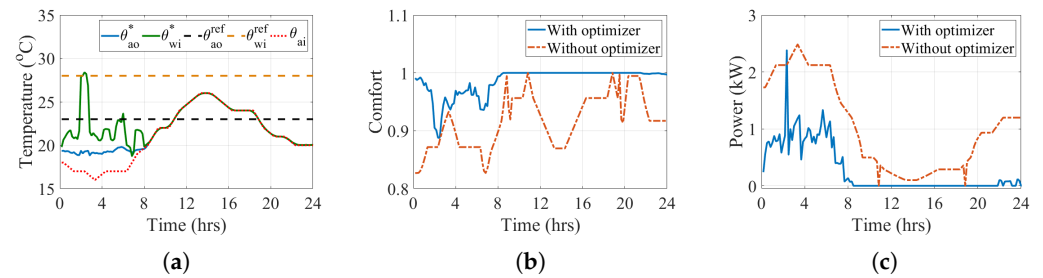


Figure 11. System performance during typical warm day in Auckland (first day of January). (a) Optimized set-points. (b) Comfort level comparison. (c) AHU system power consumption for temperature control.

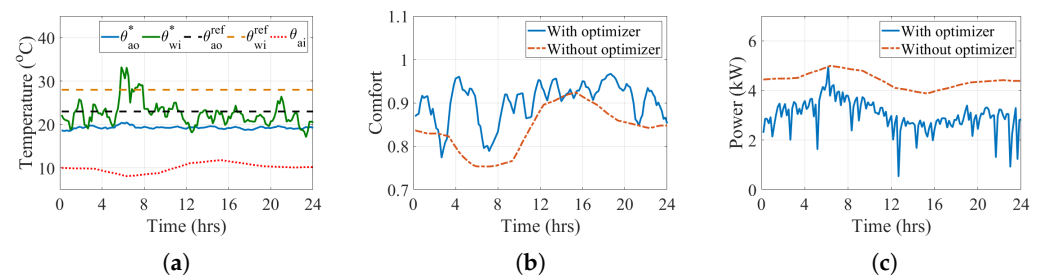


Figure 12. System performance during typical cool day in Auckland (first day of June). (a) Optimized set points. (b) Comfort level comparison. (c) AHU system power consumption for temperature control.

Note that to determine and compare the overall energy performance, the AHU plant dynamics were simulated with the conventional (see Figure 4) and proposed framework (see Figure 3) individually, considering the weather profile data for the entire year (i.e., 51,840 time steps). The corresponding AHU energy consumption E_{AHU} was evaluated as per Equation (18):

$$E_{AHU} = \sum_{q=1}^t \left(\left(\frac{1}{N_h} \sum_{k=1}^{N_h} Q_w \right) \times \Delta t \right) \quad (29)$$

where t denotes the number of hours in a considered time duration, Δt is the considered time step interval, N_h designates the number of time steps per hour and Q_w is the thermal load (i.e., AHU power consumption) at the N_h^{th} time step.

Tables 2 and 3 summarize the overall energy performance and the corresponding thermal comfort performance, respectively, provided by the AHU system. From the tables, it can be observed that the proposed control strategy could achieve annual energy savings of 49.13%, with significant improvements in the occupant thermal comfort levels.

Table 2. Overall energy performance of the AHU in kWh.

Time Duration (t)	Energy Consumption (kWh)		Energy Saving (kWh)
	Without Optimizer (E_{AHU})	With Optimizer (E_{AHU}^*)	
First Day of January (24 h)	27.41	6.49	20.92
First Day of June (24 h)	94.25	68.85	25.4
Entire Year (8640 h)	24,272.24	12,345.10	11,927.14

Table 3. Number of time steps recorded with high comfort level values.

Time Duration (N)	Number of Time Steps with Comfort Levels > 0.9		Increase in Comfort Levels (%)
	Without Optimizer (C_n)	With Optimizer (C_n^*)	
First Day of January (144 time steps)	89	136	52.80%
First Day of June (144 time steps)	26	91	250%
Entire Year (51,840 time steps)	22,869	40,090	75.30%

5.4. Computational Time Incurred by the Proposed Algorithm

Since, the proposed algorithm delivered good performance in minimizing the energy consumption and maximizing the thermal comfort, it is worthwhile to mention the computational aspect of the approach. One of the key contributions of the proposed framework in the paper is the approximation scheme, which was given in Section 3.1, for evaluating the approximate value of the outflow air temperature θ_{ao} . This was developed in particular to reduce the computation time per time step and to expedite the online optimization process.

The approximate value of θ_{ao} is given by Equation (22). This approximated value is used in the objective function $J_2(\cdot)$ of the framework (see Equation (24)). The advantage of this is that instead of generating all the AHU plant dynamics at each time step, the proposed framework uses Equation (22) to evaluate the approximate value of θ_{ao} , corresponding to the inflow air temperature θ_{ai} . This approximation technique reduced the computation time of the proposed algorithm at each time step to 0.1 s. If all the AHU plant dynamics were to be simulated during each time step, then the computational time incurred by the proposed algorithm would be 5 min (per time step). Therefore, the proposed multi-objective framework based on this approximation provides a significant improvement from the computational perspective.

5.5. Modeling Assumptions and Limitations of the Approach

The MOO framework which we developed in this study can be applied to a wide range of AHU plant models. However, the results presented above are specific to the type of AHU plant considered in this work. Thus, it makes it worthwhile to discuss some of the assumptions involved in the plant modeling and limitations of the overall approach. The AHU plant model utilized in this work was developed by adopting the lumped-capacity approach, wherein each heat exchange zone is assumed to behave as a ‘continuous stirred tank’ [29]. In other words, the heat exchange on the air side and the water side of the AHU (see Figure 1) is assumed to be instantaneous. Furthermore, a first-order representation was assumed for the control valve and actuator, which means the hysteresis due to the actuator linkage mechanism was assumed to be negligible, as mentioned in Section 2. Likewise, a first-order representation was assumed for the temperature sensor. The value of the thermal capacity of water C_w was based on the static water mass of the coil multiplied by the specific heat capacity of the water c_w , which was assumed to be constant in the model. Although the considered model was nonlinear and was experimentally verified in [29], because of the above assumptions, it is a particularly ‘idealistic’ representation of the AHU plant, and a more practical approach needs to be considered in future work. Moreover, the thermal model only considers a single output viz. the outflow air temperature θ_{ao} , and other factors which contribute towards the thermal comfort, such as humidity, were not considered as model outputs in the present work. Thus, future studies should consider evaluating the performance of the proposed MOO framework on a more versatile thermal model of the AHU plant.

6. Conclusions and Future Work

A robust control framework with meta-heuristic intelligence has been proposed, wherein the focus is on optimizing the energy performance of air handling units (AHUs) with minimal impact on thermal comfort. This is achieved by judiciously selecting the temperature set points of two controllers (i.e., the H_∞ controller and the boiler controller). The selection of these set points is formulated as a multi-objective optimization problem using a well-known meta-heuristic: Non-Dominated Sorting Genetic Algorithm-II (NSGA-II). Moreover, the uncertainty weights of the H_∞ controller are estimated to minimize the oscillations in the outflow air temperature of the AHU plant. The results of the simulation show the following:

- The two controllers (with optimal set points) could significantly reduce the oscillations in the outflow air temperature compared with the conventional case, where the temperature set points were selected empirically.
- Annual energy savings of 49.13% were achieved, with comfort levels maintained 75.3% of the time.
- The proposed multi-objective framework is computationally effective.

Thus, the proposed framework successfully achieved a balance between AHU energy consumption and thermal comfort.

For future work, as a benchmark for experimentally validating and applying the proposed framework, a miniaturized form of the AHU plant can be set up in a laboratory.

This would require the proposed framework to be written using suitable scripts on platforms such as *Python* or *C* and executed on devices such as field programmable gate arrays (FPGAs). A good starting point would be to structure the control system as per Figure 3 in an experimental set-up. Furthermore, a suitable interface could also be devised between the controller and the user for specifying the priorities of thermal comfort maximization and energy consumption minimization.

It is worth mentioning here that the overall thermal comfort is influenced by both the temperature and humidity. However, the performance of the proposed multi-objective framework in this paper was studied on a thermal model of an AHU plant, which consisted of a single output viz. the outflow air temperature. A more versatile thermal model of the AHU plant can be developed in future work, where humidity control can be considered as an additional aspect of the research.

Lastly, this work considered the usage of only NSGA-II as an optimization technique. Future work will consider the implementation of other recently proposed techniques in addition to classical optimization techniques such as MOPSO, PAES and SPEA for comprehensive performance comparison and analysis.

Author Contributions: Conceptualization, M.W., F.H. and A.S.; methodology, M.W. and F.H.; software, M.W. and F.H.; investigation, M.W.; data curation, M.W.; writing—original draft preparation, M.W.; writing—review and editing, A.S.; supervision, A.S. and A.U. All authors have read and agreed to the published version of the manuscript.

Funding: This research received no external funding.

Data Availability Statement: Not applicable.

Conflicts of Interest: The authors declare no conflict of interest.

Abbreviations

The following abbreviations are used in this manuscript:

AHU	Air handling unit
ASHRAE	American Society of Heating Refrigerating and Air-Conditioning Engineers
BEMS	Building energy management systems
HVAC	Heating, ventilation and air conditioning
HCU	Heating coil unit
MOOP	Multi-objective optimization problem
NSGA	Non-Dominated Sorting Genetic Algorithm

Nomenclature

Symbol

F	Fractional valve-stem position
A	Heating exchanger (coil) surface area
Q	Heat transfer rate
n	Integer number
g	Gain
μ	Mass-flow rate
Re	Reynolds number
Φ	Sensor output (feedback signal)
c	Specific heat capacity
θ	Temperature
C	Thermal capacity
U	Thermal transmission coefficient
τ	Time constant
d	Tube diameter
f_o	Valve let-by
\mathcal{N}	Valve authority
Ψ	Valve installed characteristics
γ	Valve inherent characteristics

Subscripts and Superscripts

<i>a</i>	Air
<i>ai</i>	Inflow air
<i>i</i>	Internal
<i>ao</i>	Outflow air
<i>pt</i>	Plant
<i>wi</i>	Inflow water
<i>wo</i>	Outflow water
<i>m</i>	Heating exchanger (coil) material
<i>s</i>	Sensor (detector)
<i>tb</i>	Tube
<i>w</i>	Water
<i>wd</i>	Water-design condition

References

- Li, D.H.; Yang, L.; Lam, J.C. Zero energy buildings and sustainable development implications—A review. *Energy* **2013**, *54*, 1–10. [CrossRef]
- Rao, D.V.; Ukil, A. Modeling of room temperature dynamics for efficient building energy management. *IEEE Trans. Syst. Man Cybern. Syst.* **2017**, *50*, 717–725. [CrossRef]
- EIA. Consumption & Efficiency. 2019. Available online: <https://www.eia.gov/consumption/> (accessed on 3 September 2019).
- Brastein, O.; Perera, D.; Pfeifer, C.; Skeie, N.O. Parameter estimation for grey-box models of building thermal behaviour. *Energy Build.* **2018**, *169*, 58–68. [CrossRef]
- Wang, Z.; Yang, R.; Wang, L. Multi-agent control system with intelligent optimization for smart and energy-efficient buildings. In Proceedings of the IECON 2010-36th Annual Conference on IEEE Industrial Electronics Society, Glendale, AZ, USA, 7–10 November 2010; pp. 1144–1149.
- Chakraborty, N.; Mondal, A.; Mondal, S. Intelligent scheduling of thermostatic devices for efficient energy management in smart grid. *IEEE Trans. Ind. Inform.* **2017**, *13*, 2899–2910. [CrossRef]
- Dounis, A.I.; Caraiosc, C. Advanced control systems engineering for energy and comfort management in a building environment—A review. *Renew. Sustain. Energy Rev.* **2009**, *13*, 1246–1261. [CrossRef]
- Široký, J.; Oldewurtel, F.; Cigler, J.; Prívar, S. Experimental analysis of model predictive control for an energy efficient building heating system. *Appl. Energy* **2011**, *88*, 3079–3087. [CrossRef]
- Wang, S.; Xu, X. Optimal and robust control of outdoor ventilation airflow rate for improving energy efficiency and IAQ. *Build. Environ.* **2004**, *39*, 763–773. [CrossRef]
- Miyata, S.; Lim, J.; Akashi, Y.; Kuwahara, Y. Optimal set-point regulation in HVAC system for controllability and energy efficiency. *Adv. Build. Energy Res.* **2020**, *14*, 160–170. [CrossRef]
- Underwood, C. Robust control of HVAC plant II: Controller design. *Build. Serv. Eng. Res. Technol.* **2000**, *21*, 63–71. [CrossRef]
- Anderson, M.; Buehner, M.; Young, P.; Hittle, D.; Anderson, C.; Tu, J.; Hodgson, D. MIMO robust control for HVAC systems. *IEEE Trans. Control Syst. Technol.* **2008**, *16*, 475–483. [CrossRef]
- Moradi, H.; Bakhtiari-Nejad, F.; Saffar-Avval, M. Multivariable robust control of an air-handling unit: A comparison between pole-placement and H_∞ controllers. *Energy Convers. Manag.* **2012**, *55*, 136–148. [CrossRef]
- Mariano-Hernández, D.; Hernández-Callejo, L.; Zorita-Lamadrid, A.; Duque-Pérez, O.; García, F.S. A review of strategies for building energy management system: Model predictive control, demand side management, optimization, and fault detect & diagnosis. *J. Build. Eng.* **2021**, *33*, 101692.
- Mansy, H.; Kwon, S. Optimal HVAC Control for Demand Response via Chance-Constrained Two-Stage Stochastic Program. *IEEE Trans. Smart Grid* **2020**, *12*, 2188–2200. [CrossRef]
- Yu, L.; Jiang, T.; Zou, Y. Online energy management for a sustainable smart home with an HVAC load and random occupancy. *IEEE Trans. Smart Grid* **2017**, *10*, 1646–1659. [CrossRef]
- Ma, K.; Hu, G.; Spanos, C.J. Energy management considering load operations and forecast errors with application to HVAC systems. *IEEE Trans. Smart Grid* **2016**, *9*, 605–614. [CrossRef]
- Lu, N. An evaluation of the HVAC load potential for providing load balancing service. *IEEE Trans. Smart Grid* **2012**, *3*, 1263–1270. [CrossRef]
- Jindal, A.; Kumar, N.; Rodrigues, J.J. A heuristic-based smart HVAC energy management scheme for university buildings. *IEEE Trans. Ind. Inform.* **2018**, *14*, 5074–5086. [CrossRef]
- Wang, Z.; Wang, L.; Dounis, A.I.; Yang, R. Multi-agent control system with information fusion based comfort model for smart buildings. *Appl. Energy* **2012**, *99*, 247–254. [CrossRef]
- Manic, M.; Wijayasekara, D.; Amarasinghe, K.; Rodriguez-Andina, J.J. Building energy management systems: The age of intelligent and adaptive buildings. *IEEE Ind. Electron. Mag.* **2016**, *10*, 25–39. [CrossRef]
- Tsui, K.M.; Chan, S.C. Demand response optimization for smart home scheduling under real-time pricing. *IEEE Trans. Smart Grid* **2012**, *3*, 1812–1821. [CrossRef]

23. Rezaei, E.; Dagdougui, H. Optimal real-time energy management in apartment building integrating microgrid with multi-zone HVAC control. *IEEE Trans. Ind. Inform.* **2020**, *16*, 6848–6856. [[CrossRef](#)]
24. Shakouri, H.; Kazemi, A. Multi-objective cost-load optimization for demand side management of a residential area in smart grids. *Sustain. Cities Soc.* **2017**, *32*, 171–180. [[CrossRef](#)]
25. Li, D.; Chiu, W.Y.; Sun, H.; Poor, H.V. Multiobjective optimization for demand side management program in smart grid. *IEEE Trans. Ind. Inform.* **2017**, *14*, 1482–1490. [[CrossRef](#)]
26. Chiu, W.Y.; Yen, G.G.; Juan, T.K. Minimum Manhattan distance approach to multiple criteria decision making in multi-objective optimization problems. *IEEE Trans. Evol. Comput.* **2016**, *20*, 972–985. [[CrossRef](#)]
27. Hafiz, F.; Swain, A.; Mendes, E.M.A.M.; Aguirre, L.A. MultiObjective Evolutionary Approach to Grey-Box Identification of Buck Converter. *IEEE Trans. Circuits Syst. I Regul. Pap.* **2020**, *67*, 2016–2028. [[CrossRef](#)]
28. Hafiz, F.; Swain, A.; Mendes, E. Multi-objective evolutionary framework for non-linear system identification: A comprehensive investigation. *Neurocomputing* **2020**, *386*, 257–280. [[CrossRef](#)]
29. Underwood, C. Robust control of HVAC plant I: Modelling. *Build. Serv. Eng. Res. Technol.* **2000**, *21*, 53–61. [[CrossRef](#)]
30. Zajic, I.; Larkowski, T.; Sumislawska, M.; Burnham, K.J.; Hill, D. Modelling of an air handling unit: A Hammerstein-bilinear model identification approach. In Proceedings of the 2011 21st International Conference on Systems Engineering, Washington, DC, USA, 16–18 August 2011; pp. 59–63.
31. Deb, K. Multi-objective optimisation using evolutionary algorithms: An introduction. In *Multi-Objective Evolutionary Optimisation for Product Design and Manufacturing*; Springer: Berlin/Heidelberg, Germany, 2011; pp. 3–34.
32. Deb, K.; Pratap, A.; Agarwal, S.; Meyarivan, T. A fast and elitist multiobjective genetic algorithm: NSGA-II. *IEEE Trans. Evol. Comput.* **2002**, *6*, 182–197. [[CrossRef](#)]
33. Pang, L.M.; Ishibuchi, H.; Shang, K. NSGA-II with simple modification works well on a wide variety of many-objective problems. *IEEE Access* **2020**, *8*, 190240–190250. [[CrossRef](#)]
34. Jain, A.; Lalwani, S.; Lalwani, M. A comparative analysis of MOPSO, NSGA-II, SPEA2 and PESA2 for multi-objective optimal power flow. In Proceedings of the 2018 2nd International Conference on Power, Energy and Environment: Towards Smart Technology (ICEPE), Shillong, India, 1–2 June 2018; pp. 1–6.
35. National Institute of Water and Atmospheric Research Limited (NIWA). Weather and Climate Forecasting Services, Auckland, New Zealand. 2021. Available online: <https://niwa.co.nz/our-services/online-services/environmental-data-explorer-new-zealand> (accessed on 25 December 2022).
36. ASHRAE. *ASHRAE STANDARD: Thermal Environmental Conditions for Human Occupancy*; ASHRAE: Peachtree Corners, GA, USA, 2016; ISSN 1041-2336.

Disclaimer/Publisher’s Note: The statements, opinions and data contained in all publications are solely those of the individual author(s) and contributor(s) and not of MDPI and/or the editor(s). MDPI and/or the editor(s) disclaim responsibility for any injury to people or property resulting from any ideas, methods, instructions or products referred to in the content.